Supplement of Atmos. Chem. Phys. Discuss., 15, 9815–9895, 2015
http://www.atmos-chem-phys-discuss.net/15/9815/2015/
doi:10.5194/acpd-15-9815-2015-supplement
© Author(s) 2015. CC Attribution 3.0 License.

Atmospheric Chemistry and Physics Discussions
Open Access

Supplement of

Development and optimization of a wildfire plume rise model based on remote sensing data inputs – Part 2

R. Paugam et al.

Correspondence to: R. Paugam (ronan.paugam@kcl.ac.uk)

1 Optimization of the PRMv2 model using the Markov chain Monte Carlo algorithm:

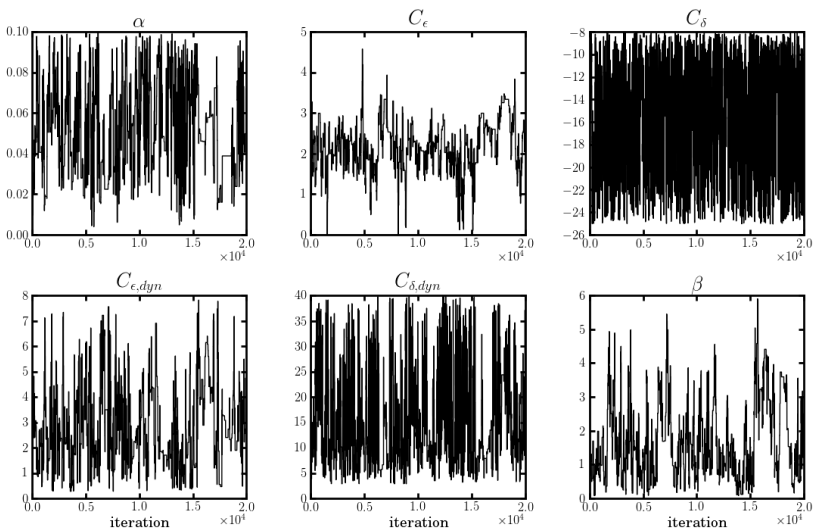

Figure S1: McMC parameters chain.

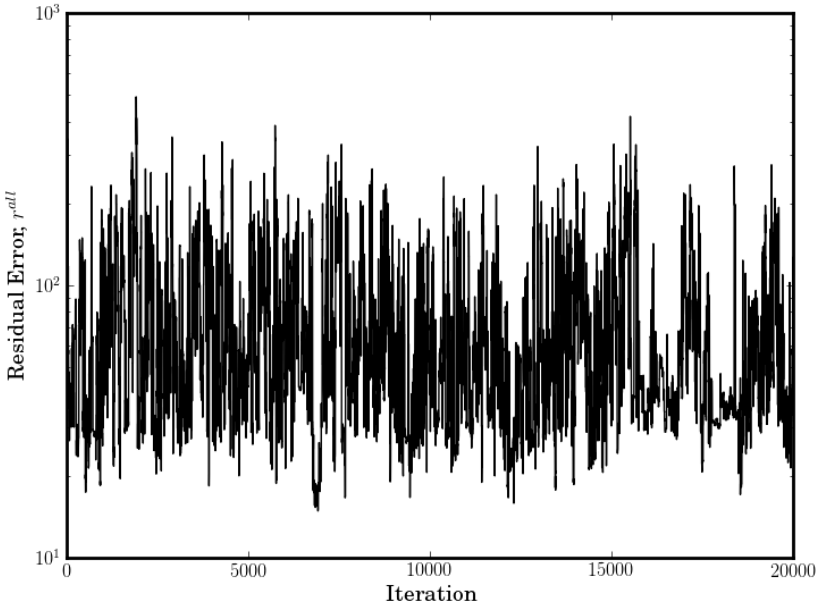

Figure S2: McMC residual error r^{all} chain.

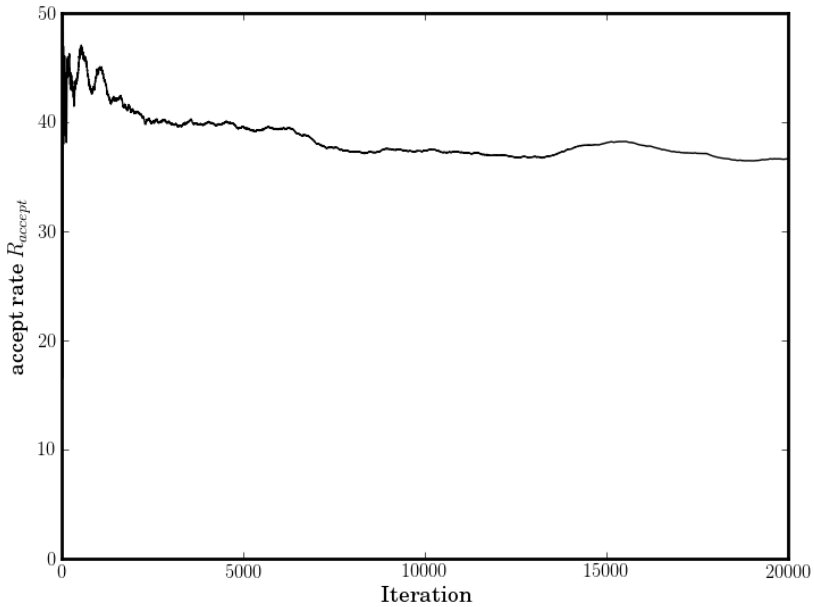

Figure S3: McMC acceptance Rate R_{accept} chain.

2 Spatial distribution of InjH for Summer 2003 over North America modelled with PRMv0, PRMv1, and the Sofiev parameterization

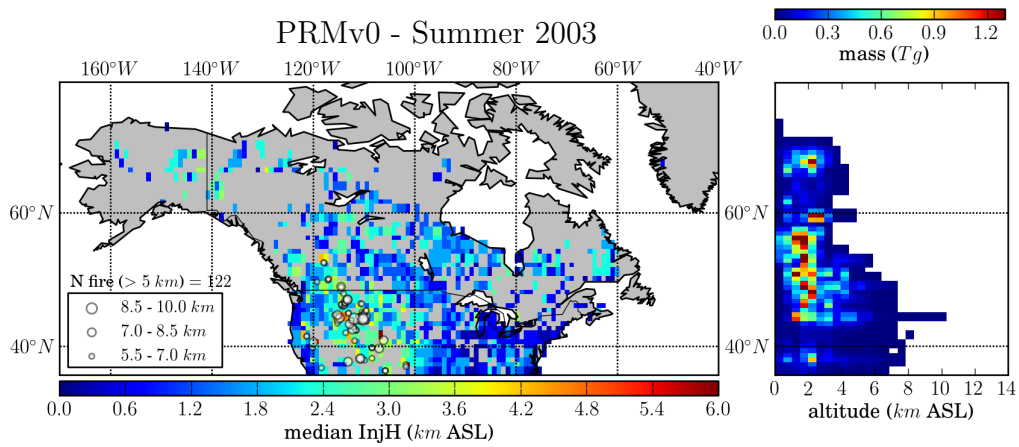

Figure S4: Seasonal maps of InjH distribution over North America for the year 2003. Fires occurrence is based on the collection 5 of the Moderate-resolution Imaging Spectroradiometer (MODIS) active fire product, and a simple model of $6h$ persistence is used to model fire evolution. InjH is modelled with the PRMv0 model and gridded on a 1.0^o resolution map with a 500 m vertical grid resolution. For each season, horizontal distribution of the seasonal integrated InjH median (left plot), single fire events with a modelled plume above 5 km (left plot), and vertical burnt mass distribution integrated over the longitude (right plot) are shown.

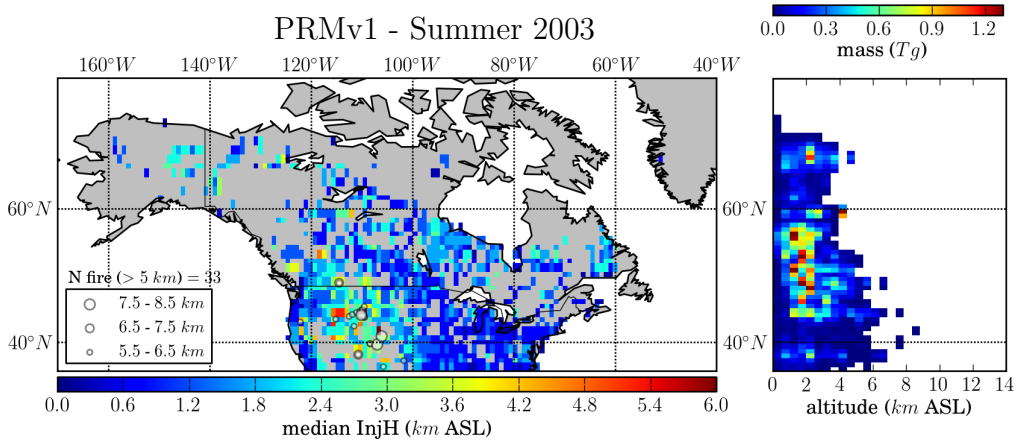

Figure S5: same as for Figure S4, but using the model PRMv1.

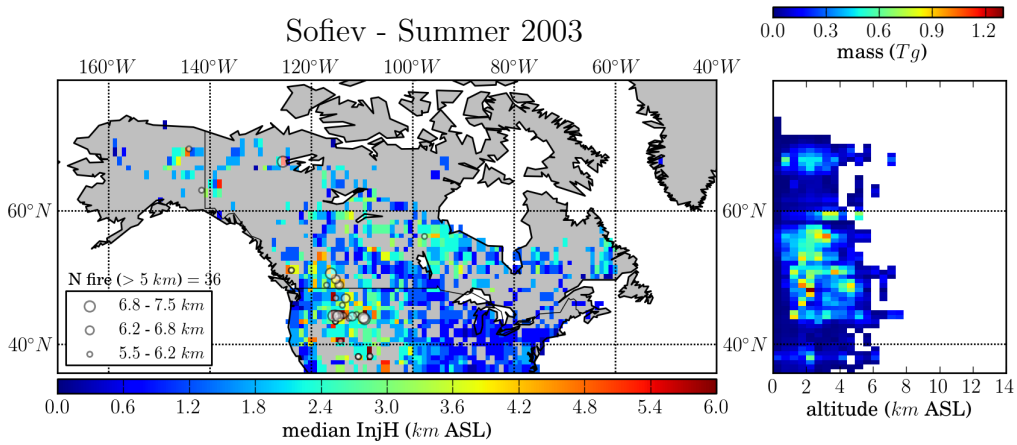

Figure S6: same as for Figure S4, but using the sofiev parameterization.

3 Time evolution of the 38 "good" fire dataset defined in Section 4.2

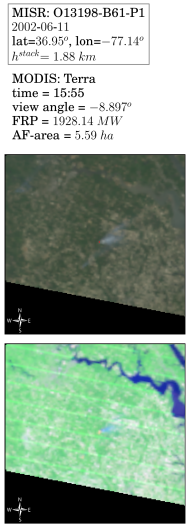

Figure S7: Time evolution of the fire O13198-B61-P1 from the Multi-angle Imaging SpectroRadiometer (MISR) plume height project. Observation are made of all available overpasses form the Moderate-resolution Imaging Spectroradiometer (MODIS) sensors on board the Terra and Aqua satellite. For each overpass (i) FRP and AF-area are computed from the Dozier Algorithm (See Section 3.2 of the manuscript), (ii) a false-color composite image is made from the MODIS MODIS bands 0.6 (red,R), 0.55 (green,G) and 0.47 μm (blue,B) and geo-reference on a 100x100 km^2 grid with a 1 km resolution around the location of the MISR detected fire; fire pixel from the collection 5 MODIS active fire product are also reported with the following color code, black: sub-pixel temperature < 600 K, red: sub-pixel temperature > 600 K and part of the fire cluster with the highest FRP, green: sub-pixel temperature > 600 K other and part of another fire cluster, (iii) and a Near-Infra Read (NIR) composite images formed of the MODIS band R=2.15, G=1.24, B=0.6 μm. See manuscript for an explanation of the NIR composite image colors.

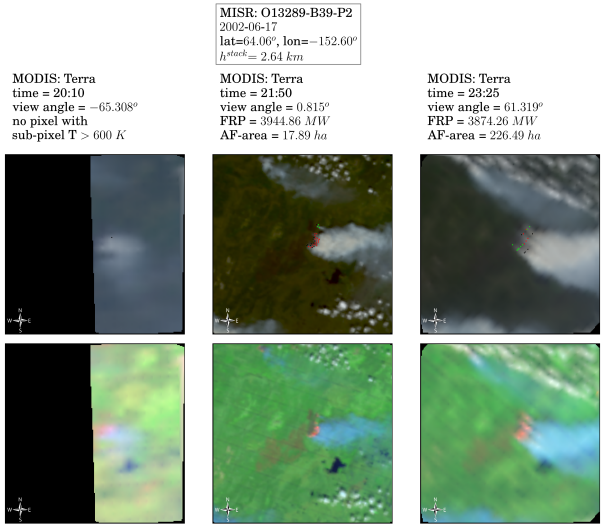

Figure S8: Time evolution of the fire O13289-B39-P2. See caption of Figure S7 for more details.

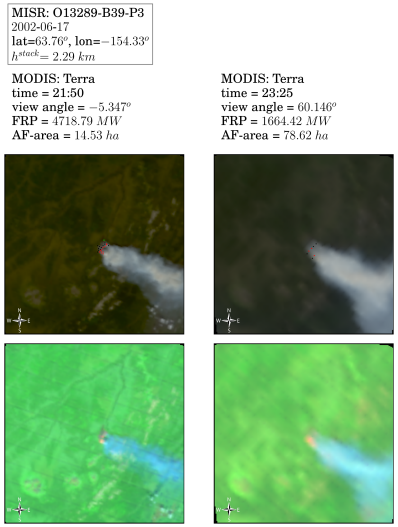

Figure S9: Time evolution of the fire O13289-B39-P3. See caption of Figure S7 for more details.

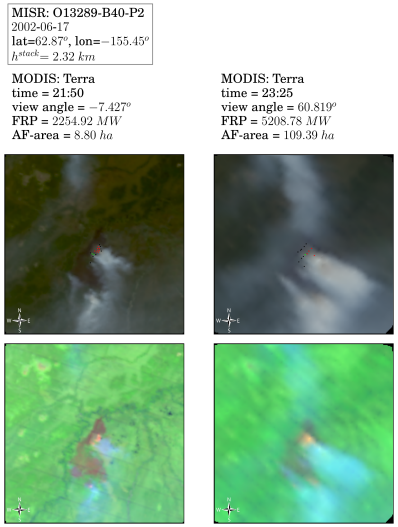

Figure S10: Time evolution of the fire O13289-B40-P2. See caption of Figure S7 for more details.

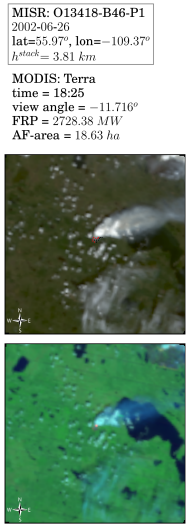

Figure S11: Time evolution of the fire O13418-B46-P1. See caption of Figure S7 for more details.

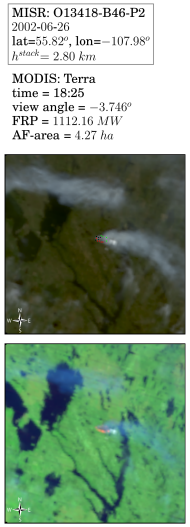

Figure S12: Time evolution of the fire O13418-B46-P2. See caption of Figure S7 for more details.

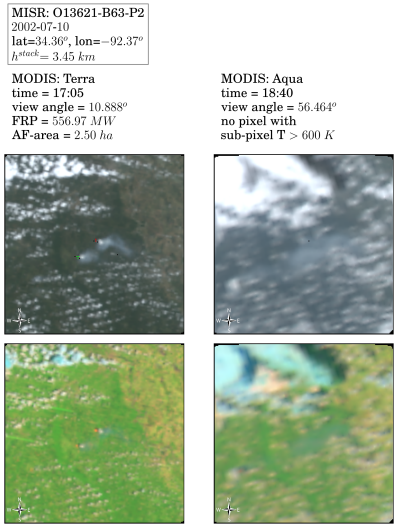

Figure S13: Time evolution of the fire O13621-B63-P2. See caption of Figure S7 for more details.

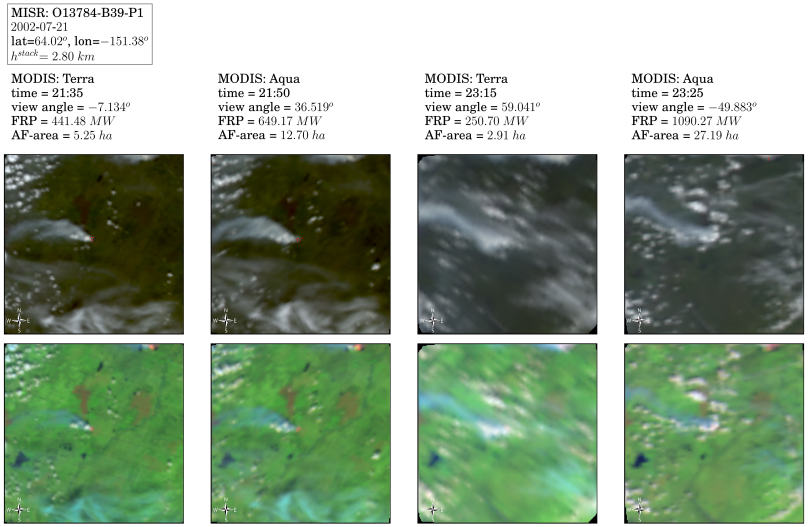

Figure S14: Time evolution of the fire O13784-B39-P1. See caption of Figure S7 for more details.

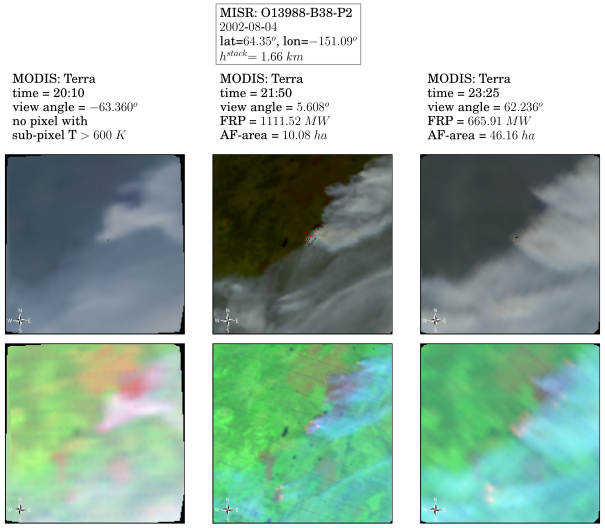

Figure S15: Time evolution of the fire O13988-B38-P2. See caption of Figure S7 for more details.

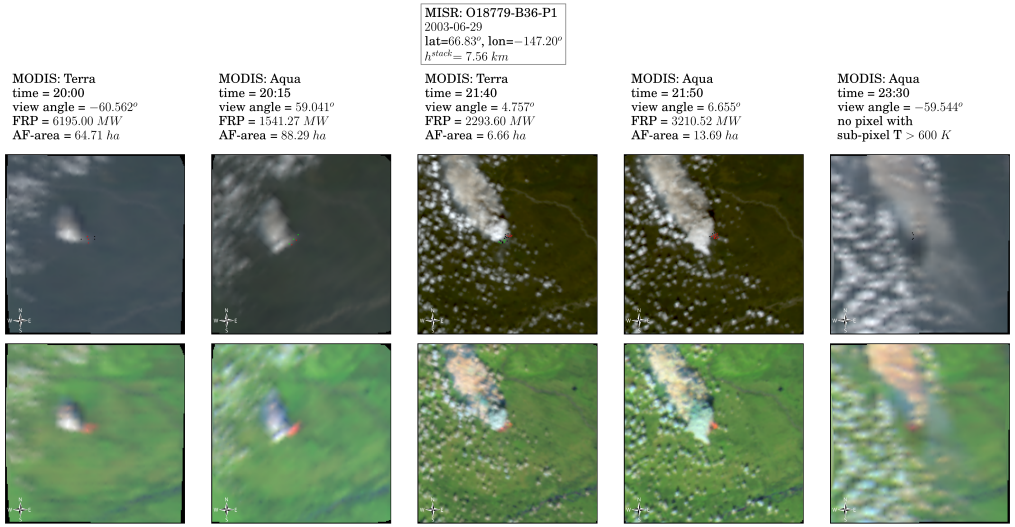

Figure S16: Time evolution of the fire O18779-B36-P1. See caption of Figure S7 for more details.

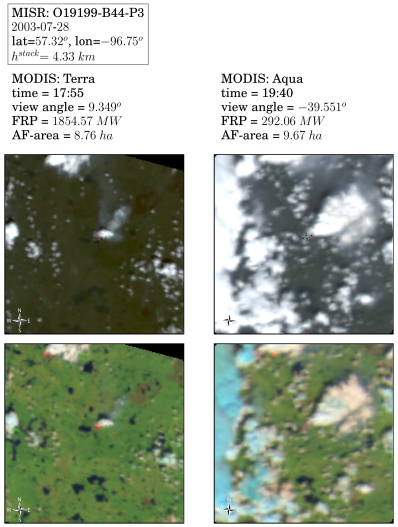

Figure S17: Time evolution of the fire O19199-B44-P3. See caption of Figure S7 for more details.

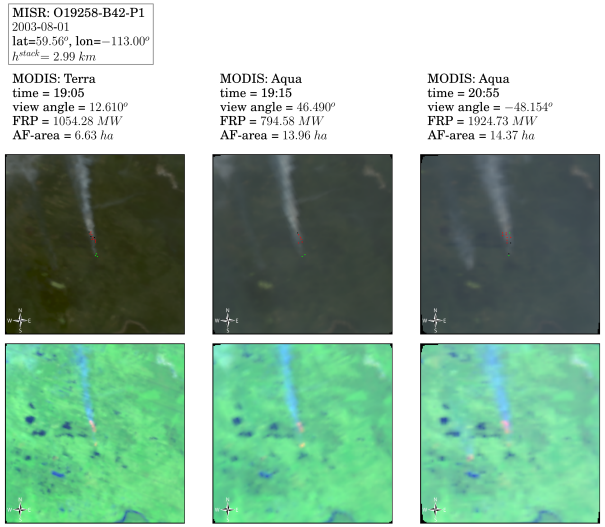

Figure S18: Time evolution of the fire O19258-B42-P1. See caption of Figure S7 for more details.

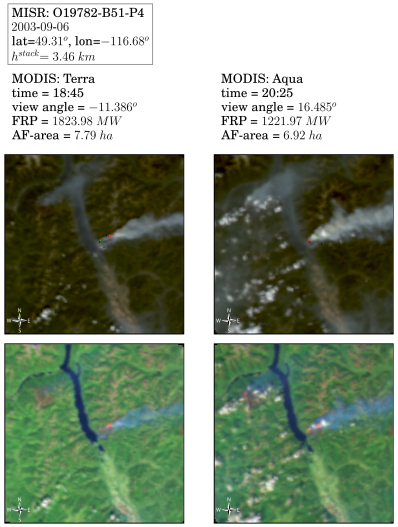

Figure S19: Time evolution of the fire O19782-B51-P4. See caption of Figure S7 for more details.

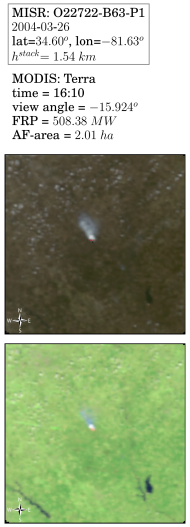

Figure S20: Time evolution of the fire O22722-B63-P1. See caption of Figure S7 for more details.

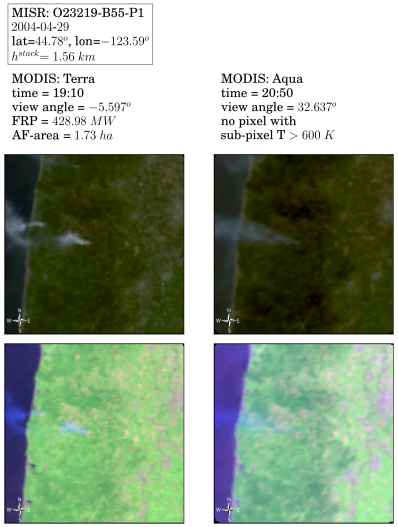

Figure S21: Time evolution of the fire O23219-B55-P1. See caption of Figure S7 for more details.

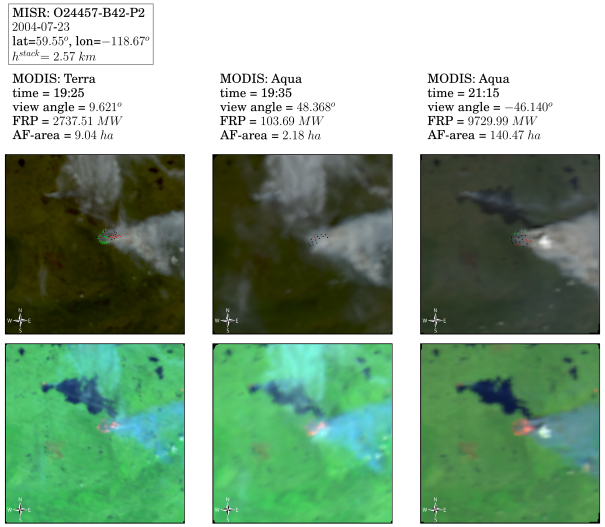

Figure S22: Time evolution of the fire O24457-B42-P2. See caption of Figure S7 for more details.

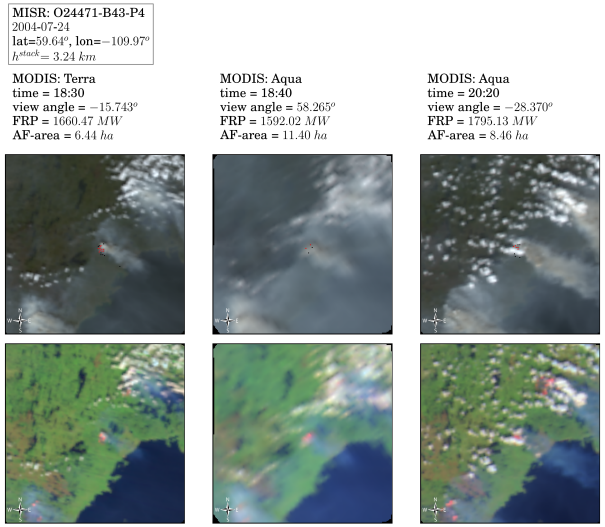

Figure S23: Time evolution of the fire O24471-B43-P4. See caption of Figure S7 for more details.

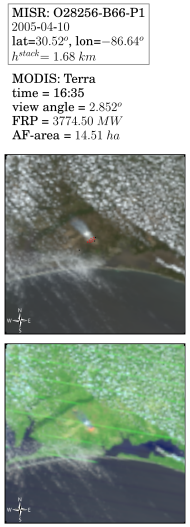

Figure S24: Time evolution of the fire O28256-B66-P1. See caption of Figure S7 for more details.

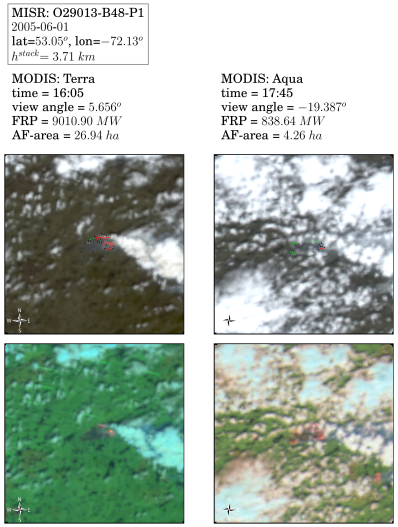

Figure S25: Time evolution of the fire O29013-B48-P1. See caption of Figure S7 for more details.

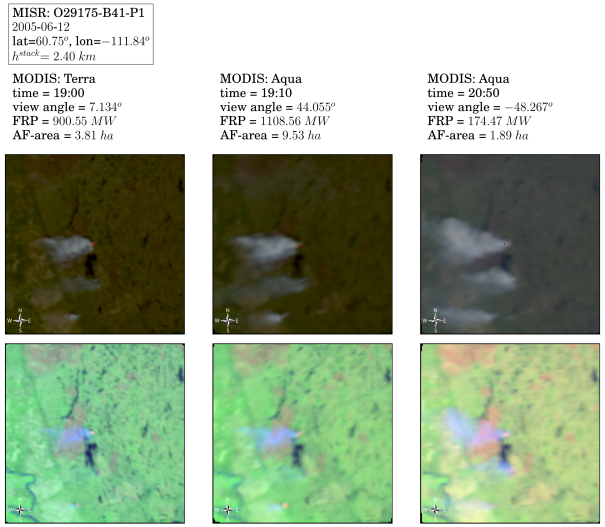

Figure S26: Time evolution of the fire O29175-B41-P1. See caption of Figure S7 for more details.

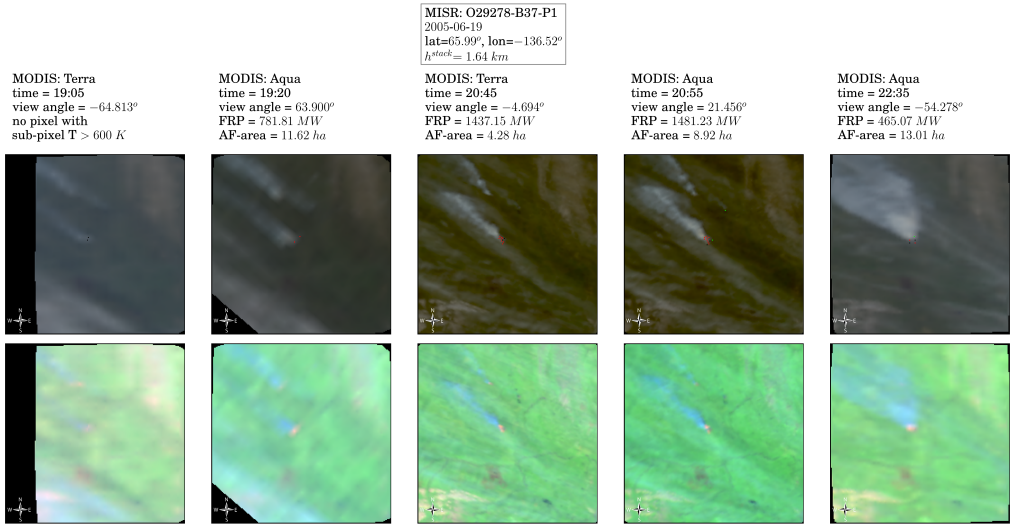

Figure S27: Time evolution of the fire O29278-B37-P1. See caption of Figure S7 for more details.

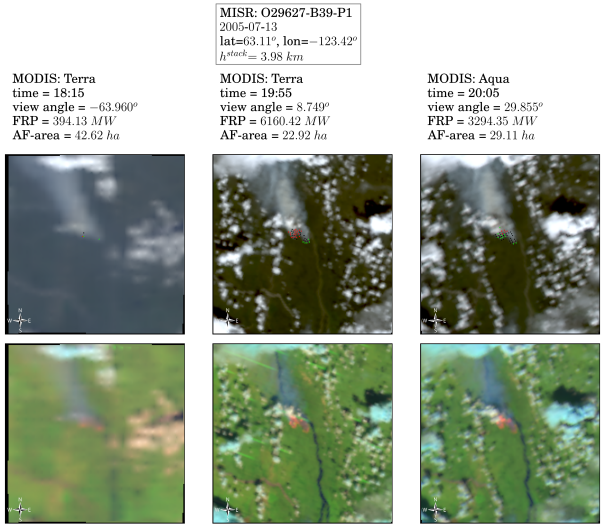

Figure S28: Time evolution of the fire O29627-B39-P1. See caption of Figure S7 for more details.

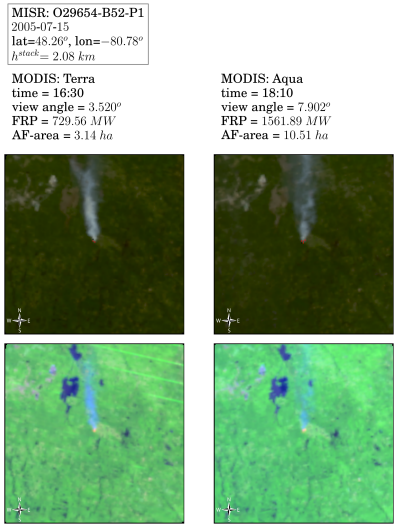

Figure S29: Time evolution of the fire O29654-B52-P1. See caption of Figure S7 for more details.

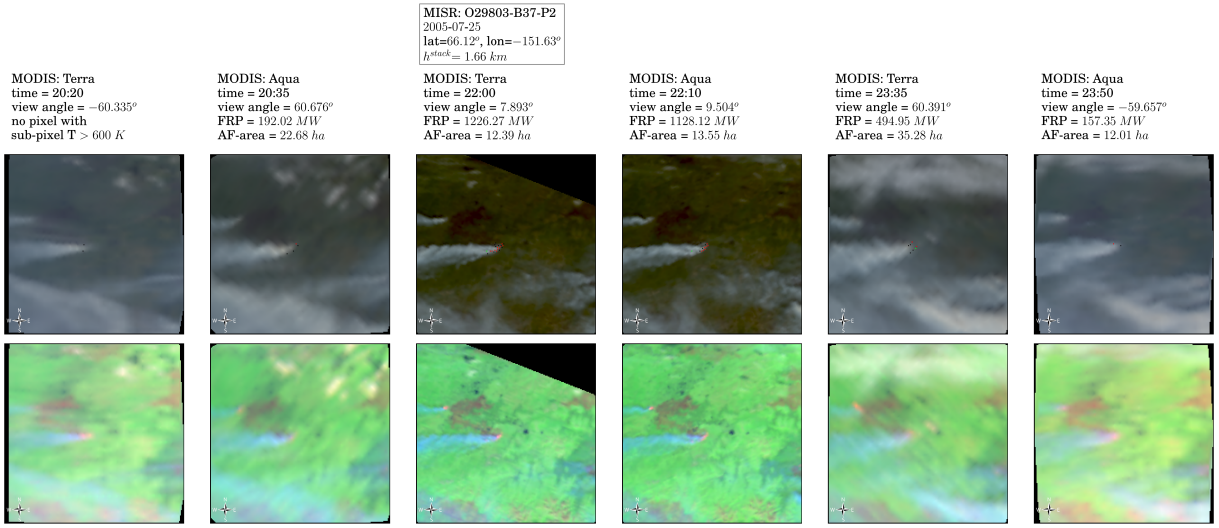

Figure S30: Time evolution of the fire O29803-B37-P2. See caption of Figure S7 for more details.

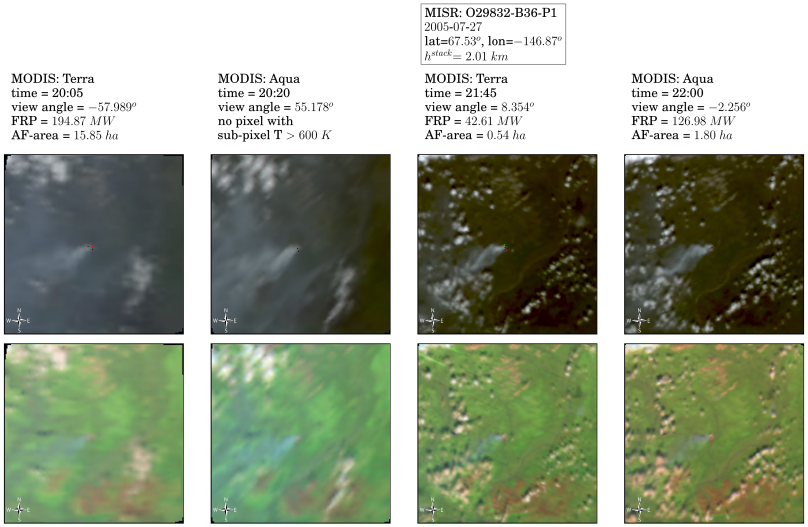

Figure S31: Time evolution of the fire O29832-B36-P1. See caption of Figure S7 for more details.

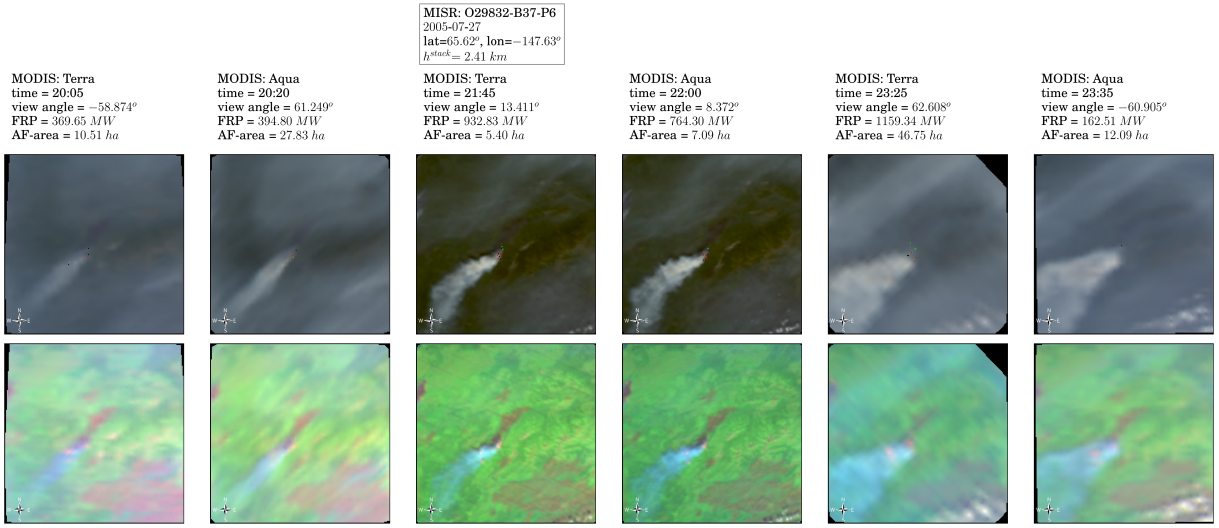

Figure S32: Time evolution of the fire O29832-B37-P6. See caption of Figure S7 for more details.

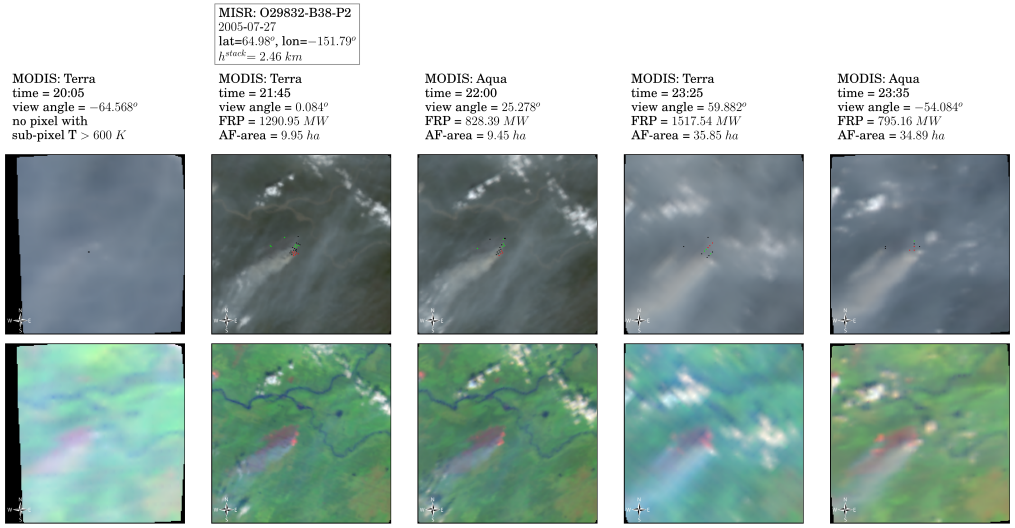

Figure S33: Time evolution of the fire O29832-B38-P2. See caption of Figure S7 for more details.

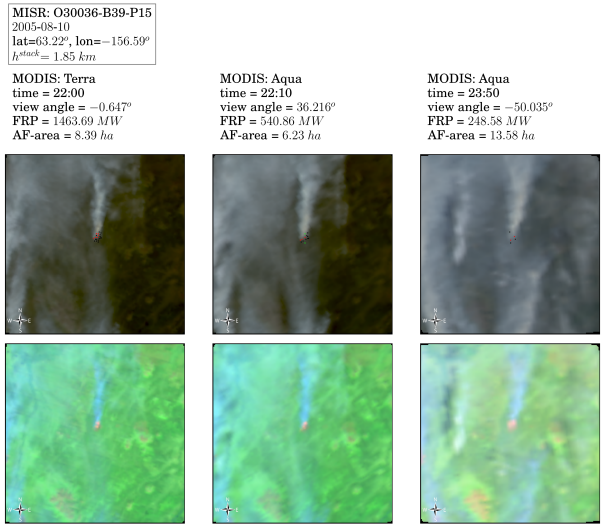

Figure S34: Time evolution of the fire O30036-B39-P15. See caption of Figure S7 for more details.

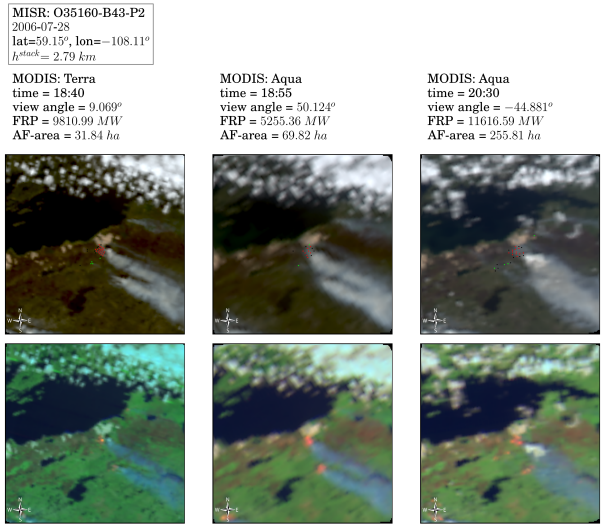

Figure S35: Time evolution of the fire O35160-B43-P2. See caption of Figure S7 for more details.

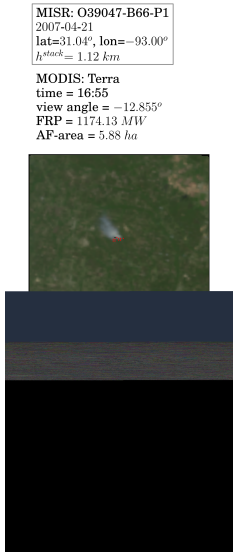

Figure S36: Time evolution of the fire O39047-B66-P1. See caption of Figure S7 for more details.

Figure S38: Time evolution of the fire O41815-B64-P3. See caption of Figure S7 for more details.

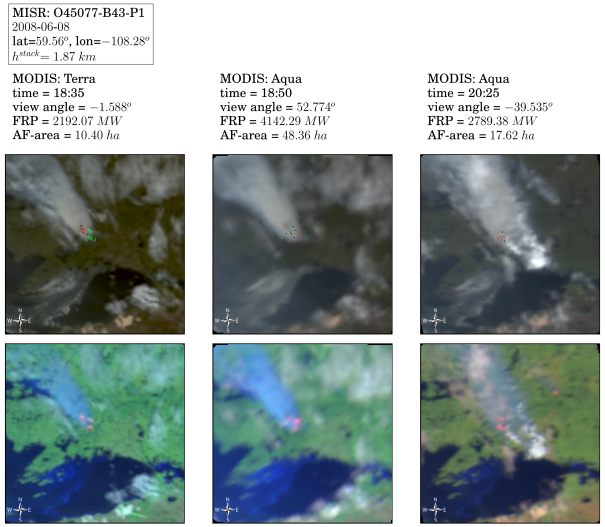

Figure S39: Time evolution of the fire O45077-B43-P1. See caption of Figure S7 for more details.

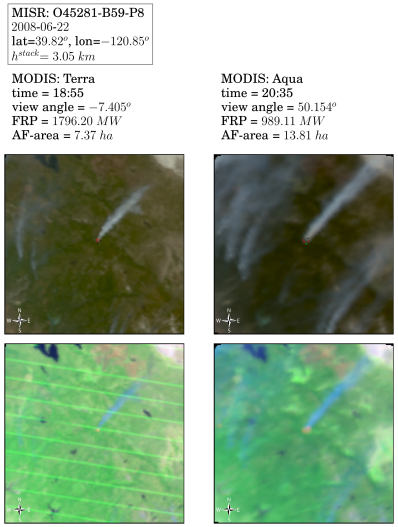

Figure S40: Time evolution of the fire O45281-B59-P8. See caption of Figure S7 for more details.

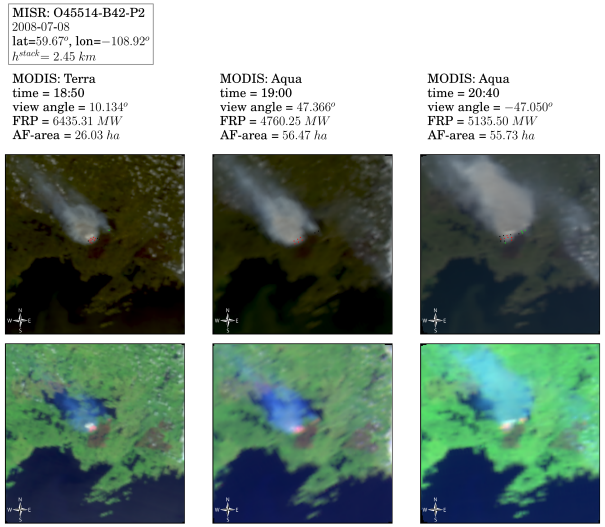

Figure S41: Time evolution of the fire O45514-B42-P2. See caption of Figure S7 for more details.

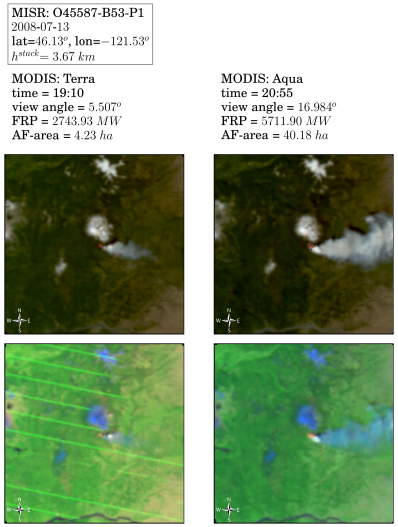

Figure S42: Time evolution of the fire O45587-B53-P1. See caption of Figure S7 for more details.

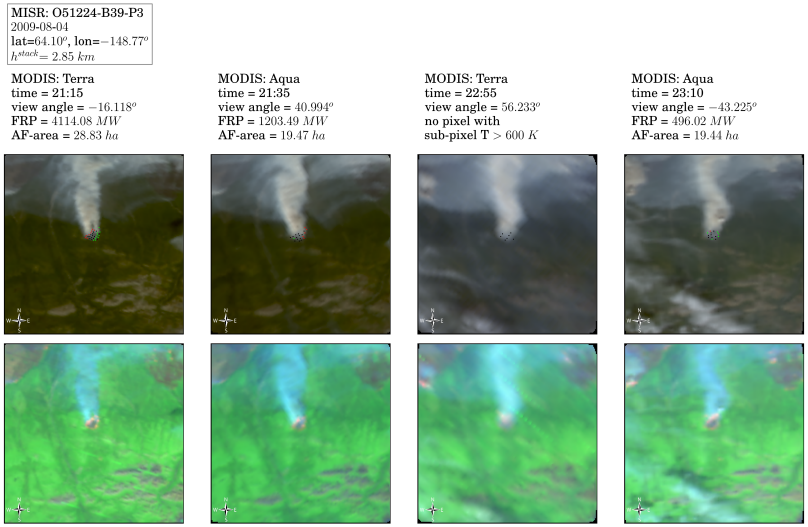

Figure S43: Time evolution of the fire O51224-B39-P3. See caption of Figure S7 for more details.

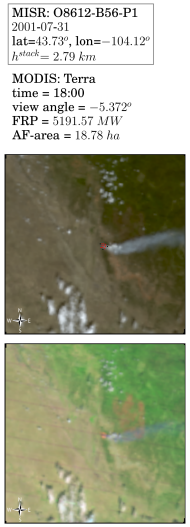

Figure S44: Time evolution of the fire O8612-B56-P1. See caption of Figure S7 for more details.

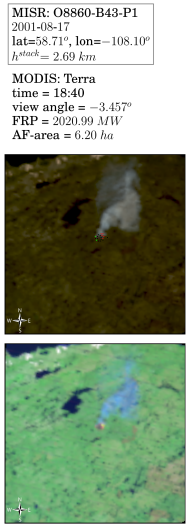

Figure S45: Time evolution of the fire O8860-B43-P1. See caption of Figure S7 for more details.